CHAPTER THREE: RESULTS

3.1 Influence of atorvastatin treatment on serum lipid metabolic parameters

Blood glucose levels and plasma levels of lipids were monitored in all of the animals studied. After STZ administration, blood glucose increased regulary to a level greater than 550 mg dl^{-1} (data not shown). Diabetic rats exhibited a threefold increase in serum triglyceride levels, a significant elevation in total cholesterol and and also a nearly threefold elevated LDL cholesterol level compared to non-diabetic controls. HDL cholesterol levels remained unchanged. Neither the increased triglyceride nor cholesterol levels in diabetic animals were influenced by the treatment with atorvastatin (Table 6).

Table 6 Metabolic characterisation on treatment day 48

	SD-Co *(*n=8)	**SD-STZ *(*n=8)**	**STZ-Ator *(*n=8)**
Triglyceride (mg dl^{-1})	1.0 ± 0.1	3.1 ± 0.5*	4.3 ± 1.0*
Total cholesterol (mg dl^{-1})	1.5 ± 0.1	2.5 ± 0.2*	2.7 ± 0.1*
LDL cholesterol (mg dl^{-1})	0.16 ± 0.05	0.47 ± 0.03*	0.5 ± 0.03*
HDL cholesterol (mg dl^{-1})	1.1 ± 0.1	1.1 ± 0.1	1.1 ± 0.1

Table 6 SD-Co indicates non-diabetic SD control rats without STZ administration. SD-STZ stands for STZ induced diabetic rats with vehicle-treatment. Diabetic rats with atorvastatin treatment are indicated by STZ-Ator. Number of animals used are in parentheses. Data are expressed as mean ± SEM. STZ injection led to enhanced lipid metabolic markers, atorvastatin treatment did not affect the level of lipid. * $P<0.05$ vs SD-Co.

3.2 Effects of atorvastatin treatment on vascular function

3.2.1 Endothelium-dependent vasodilatation

Infusion of KHS led to a flow-mediated, endothelium-dependent vasodilatation in the vascular bed of the hindlimb in every group of rats studied (Fig. 3). The grade of vasodilatation correlated to the volume applicated and produced a transistory fall of the perfusion pressure in the hindlimb circulation. Maximal vasorelaxations were achieved by application of 600 µl kg^{-1} KHS. Compared to control group, vasodilatation to KHS was significantly reduced in SD-STZ rats. At volumes of 80, 200 and 600 µl kg^{-1} KHS, the integral of perfusion pressure markedly decreased by 59.5%, 56.4% and 53.5%, respectively (P<0.05 vs SD-Co rats). The flow-mediated vasodilatatory response to KHS was significantly increased in atorvastatin-treated STZ-diabetic rats compared to vehicle-treated STZ-diabetic rats. Atorvastatin nearly restored endothelium-dependent vasodilatation (60, 200 and 600 µl kg^{-1}) at 122.2%, 74.7% and 101.1%, respectively (P<0.05 vs SD-STZ rats).

3.2.2 Endothelium-independent vasodilatation

The endothelium-independent vasodilatation was also studied by using an exogenous NO donor (SNP, 40 µg kg^{-1}) to stimulate the vascular smooth muscle cells directly. Vasodilatation caused by SNP, expressed as integral of perfusion pressure decrease, was significantly impaired in diabetic rats with 3554 ± 755 mmHg*s vs. 6602 ± 953 mmHg*s of non-diabetic control rats (-40.2%, P<0.05) (Fig. 4). Under diabetic conditions, atorvastatin administration had no significant effect on SNP-mediated vasorelexation (3951 ± 545 mmHg*s, +11.1%, P>0.05) compared to SD-STZ rats.

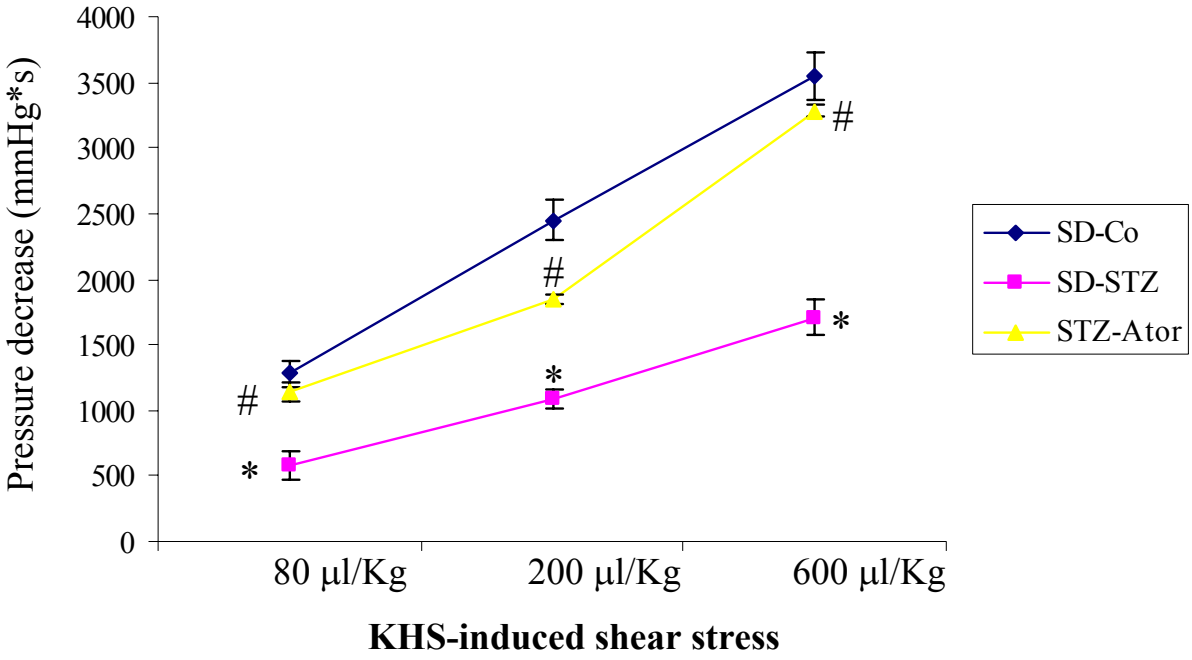

Fig. 3 Effect of atorvastatin on flow–mediated endothelium-dependent vasodilatation. Vasoactive responses were elicited by shear stress on perfusion pressure of the right hindlimb circulation, which was induced by appplication of 3 different volumes of KHS. Data are expressed as means ± SEM of the decrease of the previous pressure of the right hindlimb circulation by integral mmHg*s (n=8, each group). KHS-mediated, endothelium-dependent vasodilatation was significantly impaired in the diabetic group compared with control group. Atorvastatin increased flow-mediated, endothelium-dependent vasodilatation in the diabetic group. * P<0.05 vs SD-Co. # P<0.05 vs STZ-Ator.

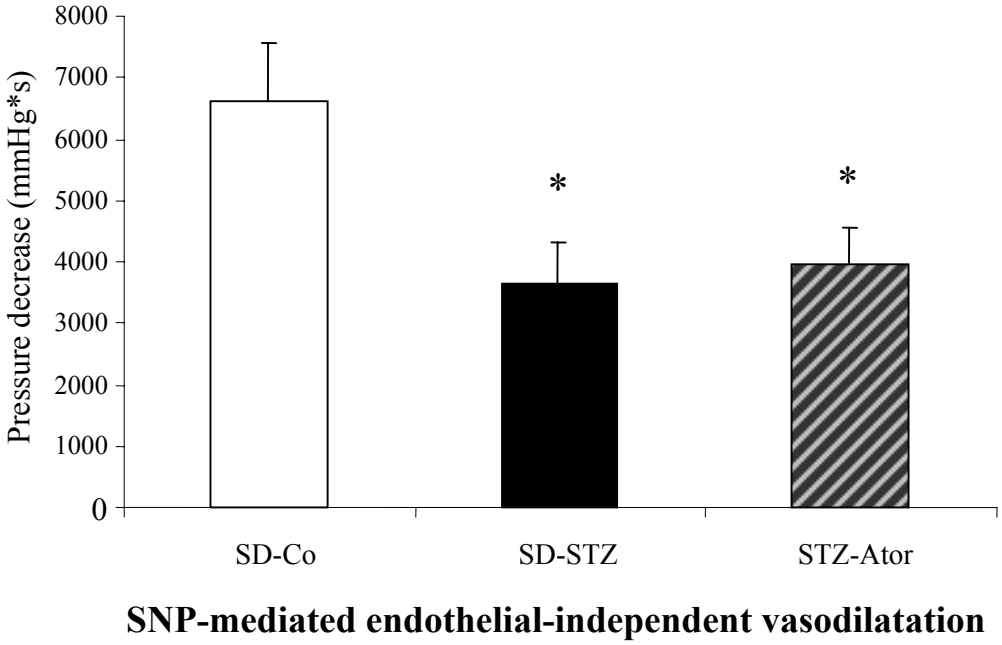

Fig. 4 Effect of atorvastatin on SNP-mediated vasodilatation. Vasoactive responses were induced by SNP (40 μg kg^{-1}) on perfusion pressure of the hindlimb circulation. SNP-mediated, endothelium-independent vasodilatation in the diabetic group was significantly impaired in diabetic group compared with control group. Atorvastatin did not significantly affect SNP-mediated vasodilatation in the diabtic group (n=8, each group). * P<0.05 vs SD-Co.

3.3 Effect of atorvastatin treatment on oxidative stress

3.3.1 NAD(P)H oxidase activity

NAD(P)H oxidase is the major resource responsible for oxidative stress under diabetic condition. NADH/NADPH oxidase activity was measured by SOD-inhibitable cytochrome *c* reduction using NADH or NADPH as substrates in the non-perfused quadriceps muscle 48 days after induction of diabetes mellitus. As shown in Fig. 5, STZ-induced diabetes significantly augmented 4-fold NADPH oxidase activity (mU mg^{-1}) ($P<0.05$), whereas treatment with atorvastatin (50 mg/kg) in diabetic rats led to a marked reduction (28%) in NAD(P)H oxidase activity compared to SD-STZ diabetic rats ($P<0.05$).

3.3.2 Expression of eNOS

Both real-time RT-PCR and Western blot were performed to evaluate the expression of eNOS in the non-perfused quadriceps muscle in 3 groups. Relative *eNOS* mRNA expression in skeletal muscles was quantified as a ratio to GAPDH. Compared with non-diabetic controls, the level of *eNOS* mRNA was significantly increased in SD-STZ rats by 2.6-fold ($P<0.05$, Fig. 6). Atorvastatin (50 mg/kg) significantly decreased *eNOS* mRNA expression level by 20% ($P<0.05$). Western blot was applied to further determine protein level of eNOS (140 kDa) in skeletal muscles. eNOS expression was shown enhanced in SD-STZ rats versus SD-Co subjects (Fig. 7, 0.6 ± 0.3 vs 1.6 ± 0.3, $P<0.05$). Atorvastatin application significantly reduced eNOS expression level in STZ-Ator subjects ($P<0.05$).

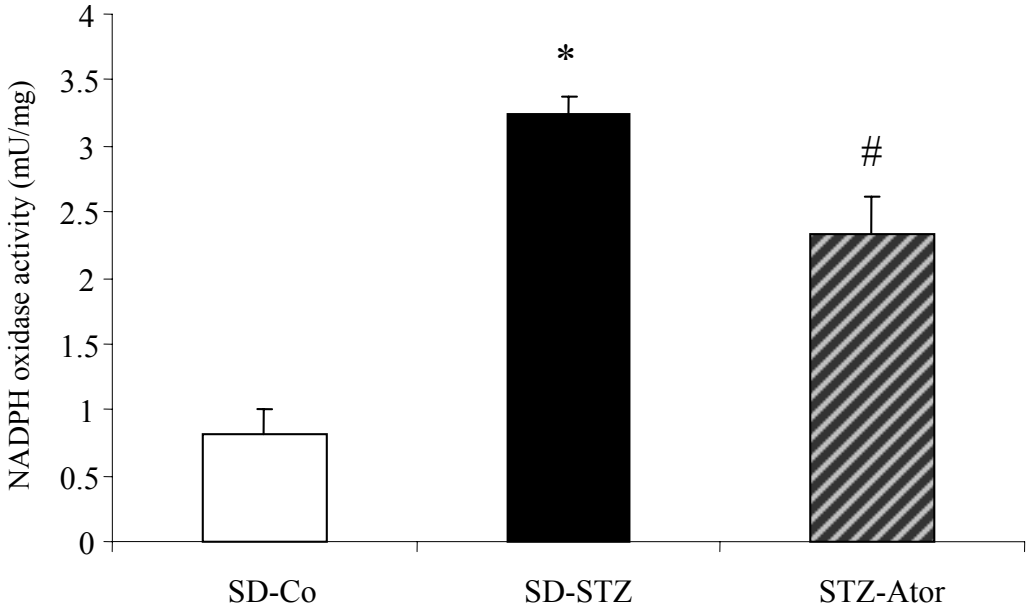

Fig. 5 Effect of Ator-treatment on NAD(P)H oxidase activity in non-perfused muscle. NAD(P)H oxidase activity was measured by SOD-inhibitable cytochrome *c* reduction using NADPH as substrate in homogenate of skeletal muscles. Data are expressed means ± SEM mU/mg (n=8, each group). * $P<0.05$ vs SD-Co. # $P<0.05$ vs SD-STZ.

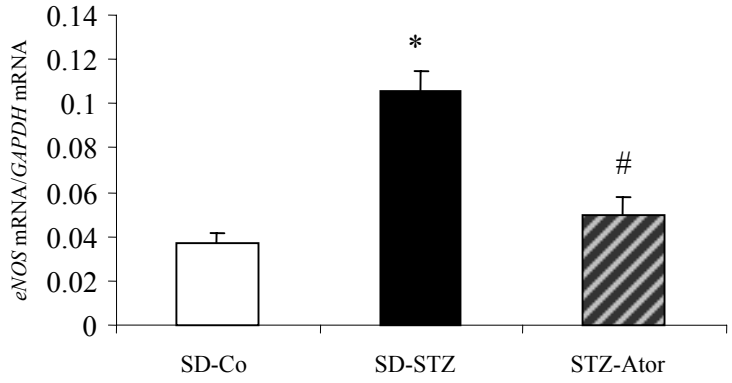

Fig. 6 Effect of atorvastatin treatment on *eNOS* mRNA expression in non-perfused muscle quantified by real-time PCR. Total RNA was isolated from the quadriceps muscles and reverse transcripted to cDNA. Ten nanogram of cDNA from each tissue sample was assayed in triplicates by real-time PCR using an ABI Prism 7000 sequence detection system, with primers and a FAM-labeled probe specific for rodent eNOS. *GAPDH* mRNA expression was used as a mRNA loading control. Relative values are normalized by GAPDH and expressed as the percentage of GAPDH. * P<0.05 vs SD-Co. # P<0.05 vs SD-STZ.

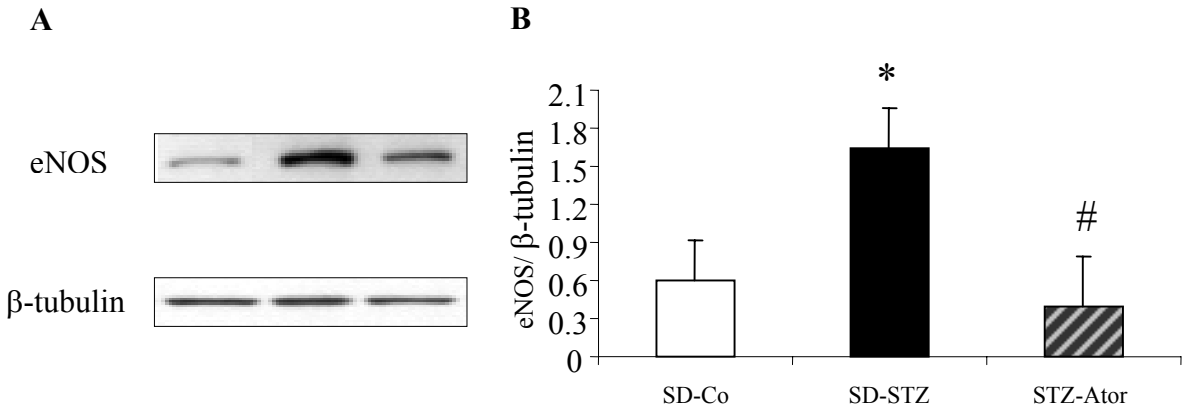

Fig. 7 Effect of atorvastatin treatment on expression of eNOS protein in non-perfused quadriceps. The expression of eNOS protein was identified by Western blotting, and the intensities of target bands (140 kDa) were quantified by densitometry. Results were normalized by β-tubulin (55 kDa) immunoblot. Representative immunoblot of eNOS was shown in A. The quantified intensities of eNOS immunoblot is shown in B, expressed as a eNOS/β-tubulin ratio. Data are presented as mean ± SEM of 5 samples in each group. * P<0.05 vs SD-Co. # P<0.05 vs SD-STZ.

3.4 Effect of atorvastatin treatment on inflammation in the non-perfused quadriceps muscle

To examine the anti-inflammatory properties of atorvastatin at a dose not affecting LDL cholesterol, expression levels of the adhesion molecules ICAM-1 and VCAM-1 and of the cytokines TNF-α and IL-1β were determined in the non-perfused quadriceps muscle at the end of the protocol. Quantification by DIA, STZ-diabetic rats demonstrated a marked increase (6-fold) in ICAM-1 protein staining compared to non-diabetic-controls (Fig. 8 D, 0.00338 ± 0.00137 vs 0.00049 ± 0.00013, $P<0.05$). The expression was localized predominantly to the endothelium (Fig. 8). Diabetic rats treated with atorvastatin exhibited a low ICAM-1 immunoreactivity, similar to this of non-diabetic controls (0.00064 ± 0.00023, $P<0.05$ vs SD-STZ rats). As shown in Fig. 9, VCAM-1 expression was also markedly increased under diabetic conditions (Fig. 9 D, 10-fold, 0.00288 ± 0.00101 vs. 0.00026 ± 0.00007, $P<0.05$) and also revealed prominent immunoreactivity localized on the endothelium (Fig. 9). As shown for ICAM-1 immunostaining, atorvastatin treatment also significantly reduced VCAM-1 protein expression (0.00074 ± 0.00037) vs SD-STZ rats.

The gene expression of *ICAM-1* mRNA, *VCAM-1* mRNA, cytokine *TNF-α* mRNA and *IL-1β* mRNA in the non-perfused quadriceps muscle were amplified and quantified by real-time RT-PCR. Relative mRNA values were normalized by and expressed as the percentage of GAPDH in Fig. 10. The result demonstrated a 4.0-fold ($P<0.001$) increase in ICAM-1 expression and a 2.5-fold ($P<0.05$) increase in VCAM-1 expression in STZ rats compared to non-diabetic animals, and confirmed the significant reduction in ICAM-1 (61%) and VCAM-1 (20%) expression respectively in STZ-Ator rats versus SD-STZ rats (Fig. 10 A). The expression of both cytokines *TNF-α* and *IL-1β* mRNA was significantly increased in STZ diabetic rats compared to SD-Co rats (Fig. 10 B, C). Administration with atorvastatin for 48 days led to a marked decrease of both inflammatory cytokines compared to SD-STZ rats: for TNF-α from 0.334 ± 0.03 to 0.138 ± 0.027; a decrease of 59% ($P<0.001$), and for IL-1β, from 0.102 ± 0.016 to 0.052 ± 0.007, a reduction of 50% ($P<0.001$).

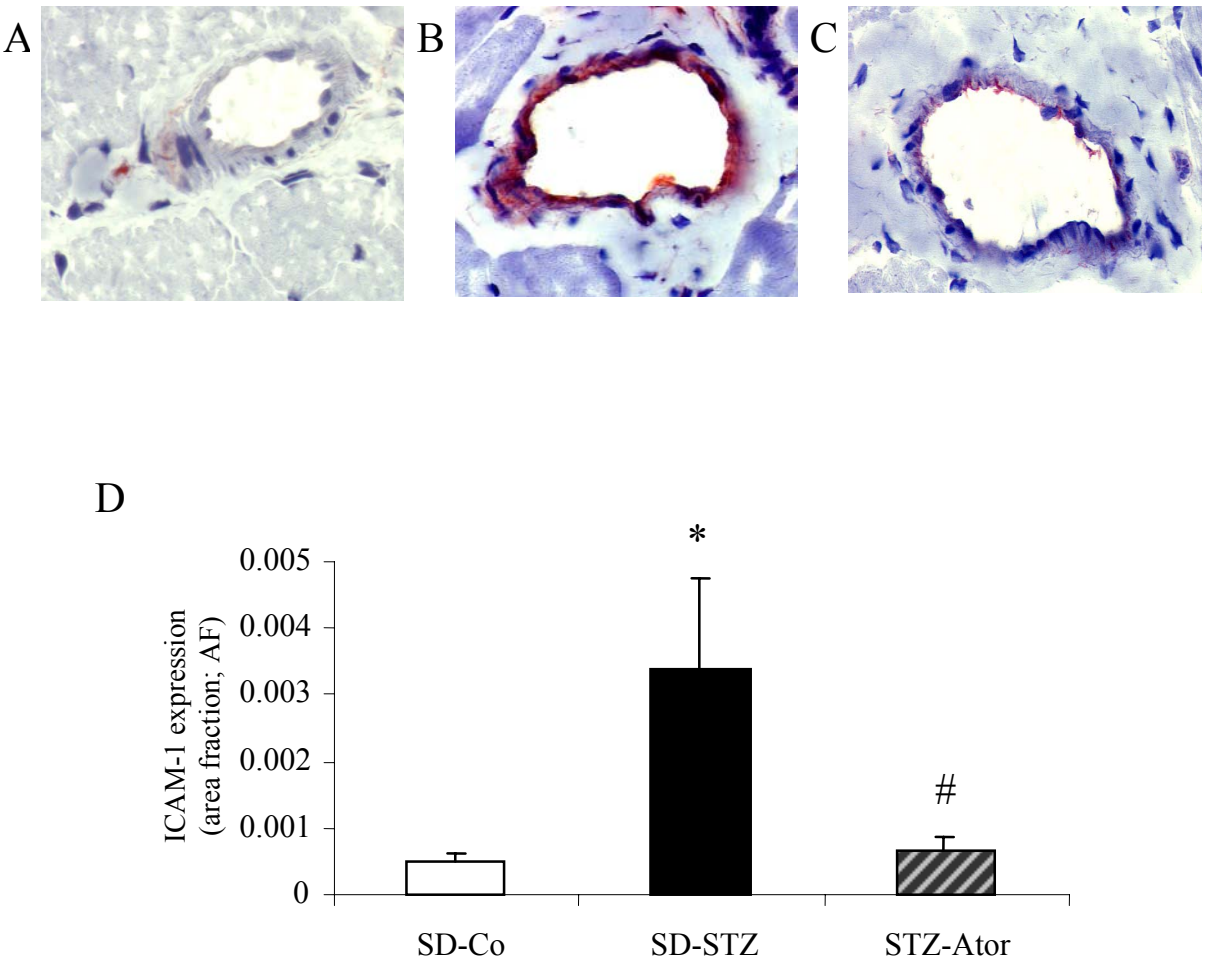

Fig. 8 ICAM-1 expression pattern in rat quadriceps muscle. Representative ICAM-1 expression was visualized with immunohistochemistry in a non-diabetic SD-Co rat (A), in a SD-STZ diabetic rat (B) and finally in an atorvastatin treated STZ-diabetic rat, STZ-Ator (C). ICAM-1 immunoreactivity, shown as red immunoprecipitate, was clearly present in the endothelium (magnification, X630). Protein expression of ICAM-1 was quantified by an image analyzer and expressed as AF [%] in D (n=6, each group). AF refers to area fraction of ICAM-1. * P<0.05 vs. SD-Co. # P<0.05 vs SD-STZ.

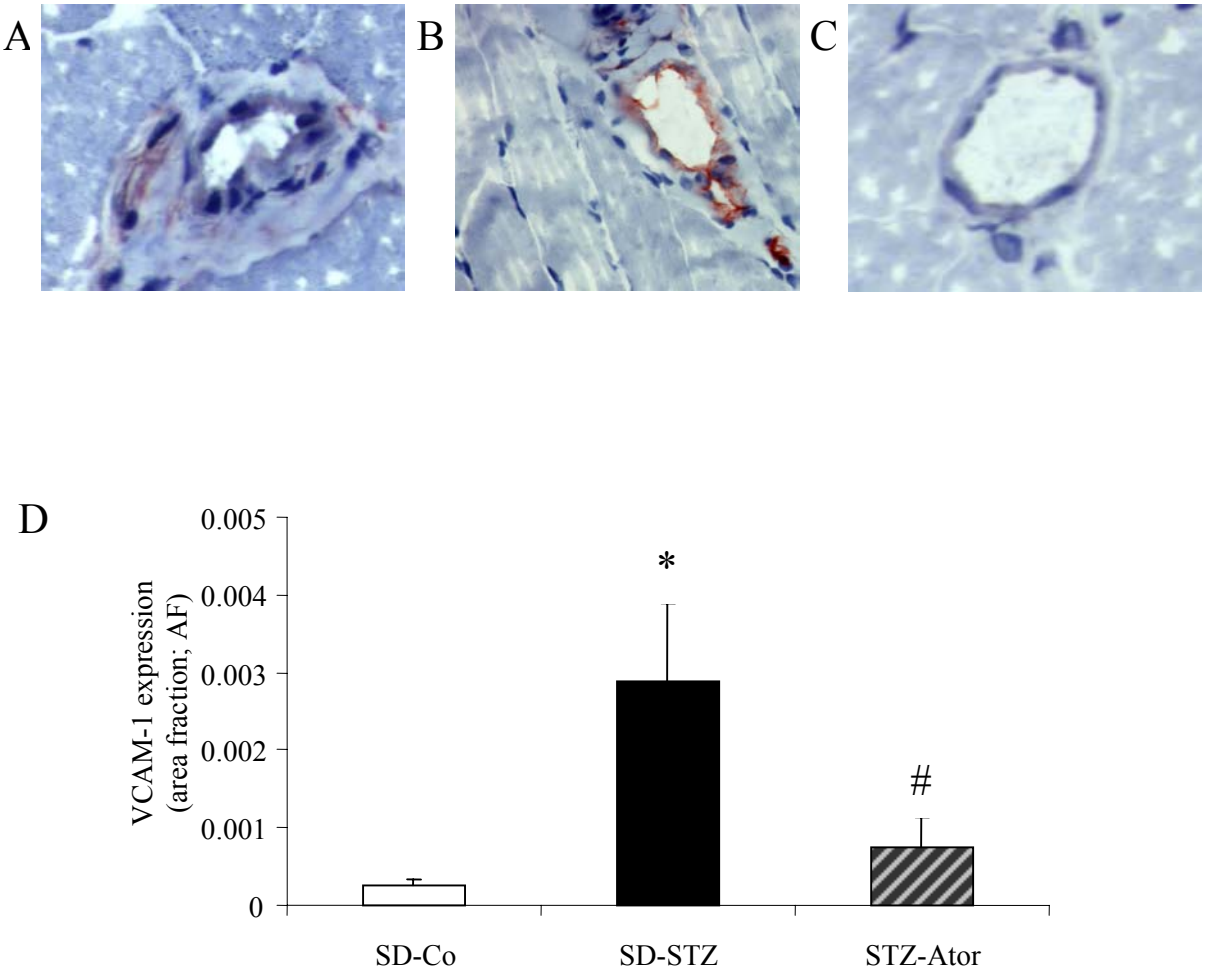

Fig. 9 VCAM-1 expression pattern in non-perfused quadriceps. Representative VCAM-1 expression was identified with immunohistochemistry in a non-diabetic SD-Co (A), in a SD-STZ diabetic rat (B) and in an atorvastatin treated STZ-diabetic rat, STZ-Ator (C). VCAM-1 immunoreactivity, which was stained as red color, was clearly present in the endothelium (magnification, X630). Protein expression of VCAM-1 was quantified by an image analyzer and expressed as AF [%] in D (n=6, each group). AF refers to area fraction of VCAM-1. * P<0.05 vs SD-Co. # P<0.05 vs SD-STZ.

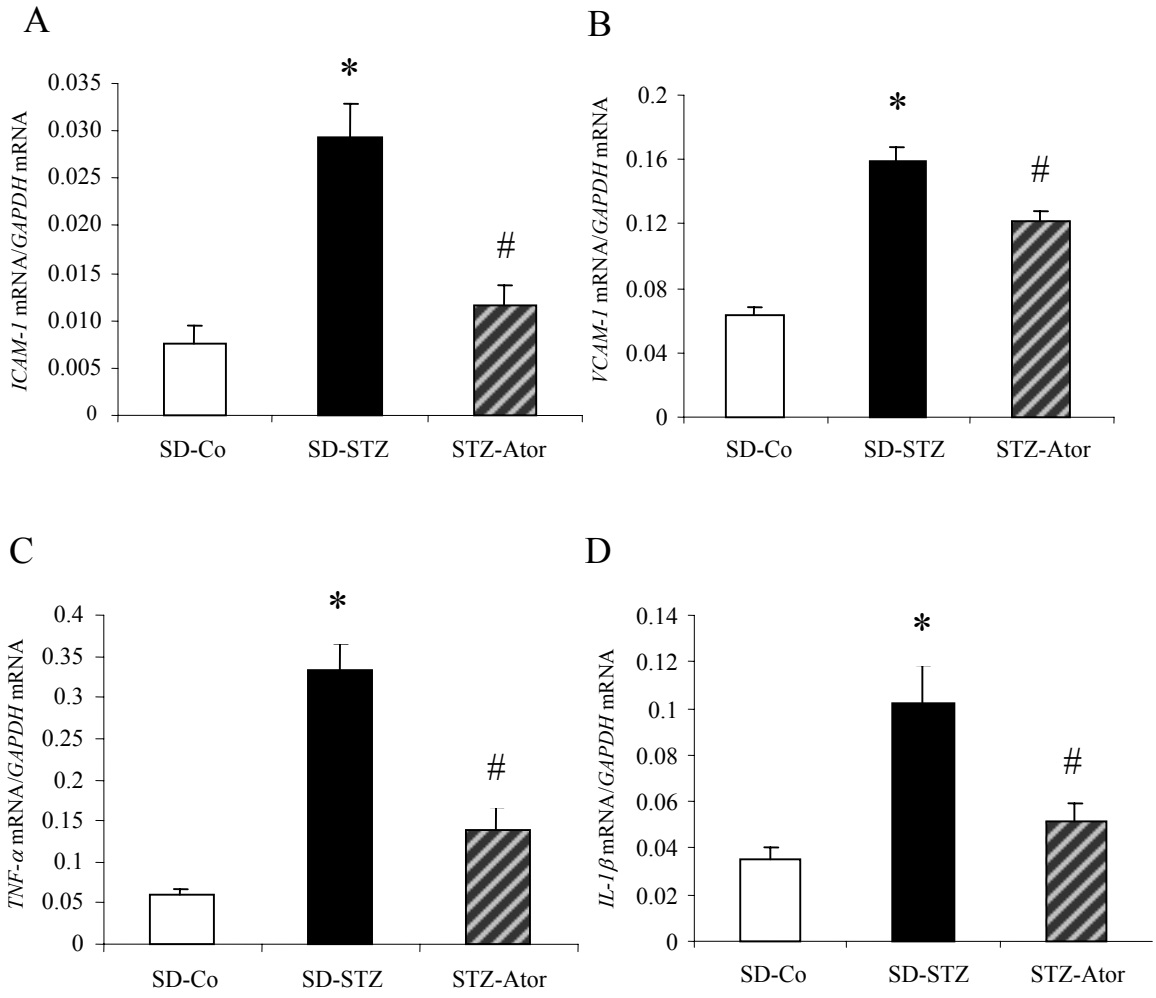

Fig. 10 Effects of Atorvastatin treatment on *ICAM-1, VCAM-1, TNF-α* and *IL-1β* mRNA expression in non-perfused muscle quantified by real-time PCR. Total RNA was isolated from the quadriceps muscles and reverse transcribed to cDNA. Ten nanogram of cDNA from each tissue sample was assayed in triplicate by real-time PCR using an ABI Prism 7000 sequence detection system, with primers and a FAM-labeled probes specific for rodent *ICAM-1*, *VCAM-1, TNF-α* and *IL-1β* mRNA. *GAPDH* mRNA expression was used as a mRNA loading control. Relative values were normalized by GAPDH and expressed as the percentage of GAPDH (n=8, each group). * $P<0.05$ vs SD-Co. # $P<0.05$ vs SD-STZ.

3.5 Effect of atorvastatin treatment on ERK 1/2 MAPK and NF-κB in the non-perfused diabetic skeletal muscles

To determine signaling pathways involved in effects atorvastatin treatment, Western blots were performed to test whether atorvastatin could alter the activity of ERK1/2 MAPK and expression of transcription factor downstream, NF-κB p65. Immunoblot analysis was employed with anti–phosphorylated ERK1/2 antibody, which recognizes phosphorylated threonine 202 and tyrosine 204 residues of p44/p42 ERK. The specific bands quantified by densitometry showed enhanced phosphorylation of ERK1/2 in diabetic rats quadriceps in Fig. 11 (original blots and quantitative densitometry). The blotting result of NF-κB p65 was shown in Fig. 12, each from five samples in the groups. STZ-induced diabets significantly increased the activity of ERK1/2 (3.8-fold of ERK1 and 2.6-fold of ERK2, respectively), which is represented by enhanced phosphorylation. The expression of NF-κB p65 level in diabetic rats were upregulated from 0.119 ± 0.032 to 1.06 ± 0.191 vs SD controls rats. The high phosphorylation of ERK1/2 evoked by STZ was significantly diminished by atorvastatin treatment, which was 67% for ERK1 and 49% for ERK2 seperately (Fig. 11). Atorvastatin administration also strikingly reduced STZ-induced NF-κB p65 over-expression (Fig. 12, -53%).

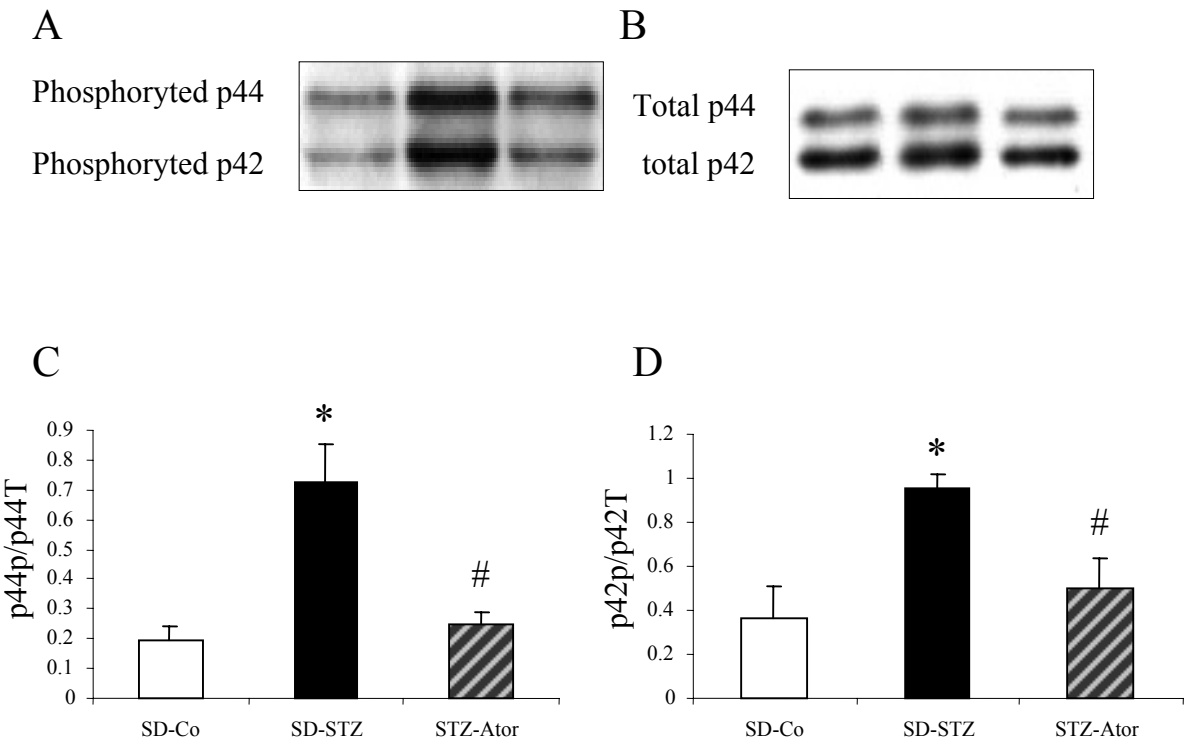

Fig. 11 Effect of atorvastatin treatment on STZ-induced ERK1/2 phosphorylation in non-perfused quadriceps. Representative immunoblots of phosphorylated ERK1/2 (phosphorylated p44 ERK and p42 ERK) (A) and total ERK1/2 (p44 ERK and p42 ERK) (B) were identified by Western blotting. After the phorsphorylated ERK1/2 antibody blotting, PVDF membranes were subsequently stripped and reprobed with ERK1/2 antibody. The specific immunoblots were quantified by densitometry. The intensities of the phosphorylated ERK1/2 and total ERK1/2 bands were expressed as an ERKp/ERKT ratio. Data obtained from quantitative densitometry are presented as mean ± SEM of 5 samples in each group. Quantified result of ERK1 (p44p/p44T) and ERK2 (p42p/p42T) are shown in C and D, respectively. * P<0.05 vs SD-Co. # P<0.05 vs SD-STZ.

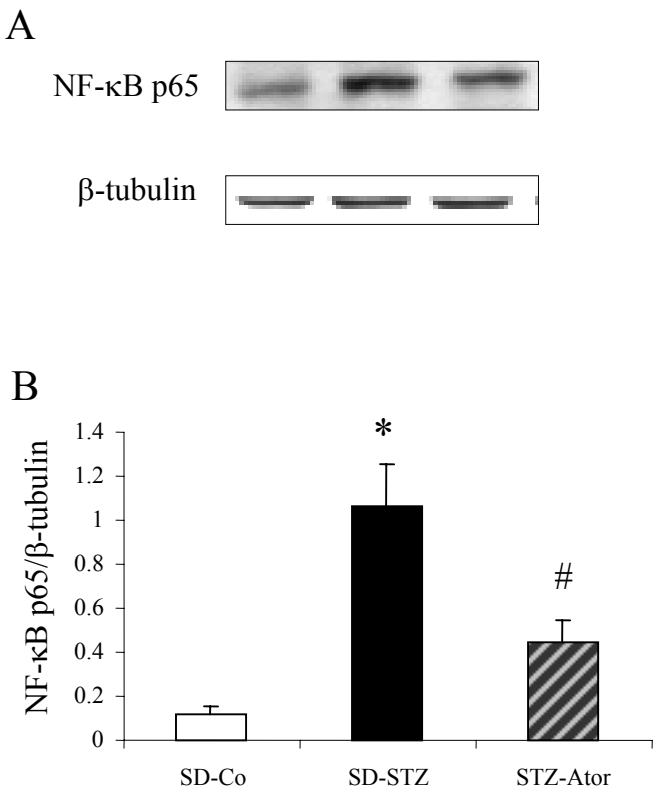

Fig. 12 Effect of atorvastatin treatment on STZ-induced NF-κB p65 expression in non-perfused quadriceps. Representative Western blots with specific bands of NF-κB p65 expression (65 kDa) is shown in A. The blots were standardized against β-tubulin. The specific immunoblots were quantified by densitometry. Densitometric quantification data are expressed as a NF-κB p65/β-tubulin ratio. Quantative data are shown in B as mean ± SEM of 5 samples in each group. * $P<0.05$ vs SD-Co, # $P<0.05$ vs STZ-Ator.